Three-dimensional, Broadband Seismometer Array Experiment at the Homestake Mine

Vuk Mandic[a], Victor C. Tsai[b], Gary L. Pavlis[c], Tanner Prestegard[a],
Daniel C. Bowden[b], Patrick Meyers[a], and Ross Caton[c]

[a] School of Physics and Astronomy, University of Minnesota, 116 Church St. SE,
Minneapolis, MN 55455, USA
[b] Seismological Laboratory, California Institute of Technology, 1200 E. California
Blvd., MS 252-21, Pasadena CA, 91125, USA.
[c] Department of Geological Sciences, Indiana University, 1001 E. 10th St.,
Bloomington, IN 47405, USA.

ABSTRACT

Seismometer deployments are often confined to near the Earth's surface for practical
reasons, despite the clear advantages of deeper seismometer installations related to lower
noise levels and more homogeneous conditions. Here, we describe a three-dimensional
(3D) broadband seismometer array deployed at the inactive Homestake Mine in South
Dakota, which takes advantage of infrastructure originally setup for mining and now used
for a range of scientific experiments. The array consists of 24 stations, of which 15 were
underground, with depths ranging from 300 feet (91 m) to 4850 feet (1478 m), and with a
3D aperture of approximately 1.5 km in each direction, thus spanning a 3D volume of
about 3.4 km^3. We describe unique opportunities and challenges related to the 3D
geometry, including the generally low ambient noise levels, the strong coherency
between observed event waveforms across the array, and the technical challenges of
running the network. This article summarizes first results and discusses directions for
potential future analysis of the Homestake array data.

INTRODUCTION

Seismology has been a ubiquitous tool for determining subsurface Earth structure and
learning about various dynamic sources, including earthquakes and nuclear explosions
[Lay and Wallace 1995; Stein and Wysession 2003]. The number of seismic arrays has
grown appreciably in the last few decades, with over 7,000 broadband seismometers
deployed within the United States alone, and over 20,000 worldwide [IRIS 2017].
However, despite this large number of seismometers, instruments have largely been
confined to the Earth's surface, with few stations having been placed at depths greater
than 100 meters, primarily due to the practical difficulty and cost of getting to such
depths. The exceptions have been limited to isolated boreholes [e.g. Abercrombie, 1995;
Ma et al., 2012], the Parkfield borehole arrays [e.g. Nadeau and McEvilly 1997), the Hi-
net array [e.g. Okada et al. 2004], and in active mines [Gibowicz et al. 1991; Richardson
and Jordan 2002). However, usually such instruments have been limited to high-
frequency geophones rather than more broadband seismometers; this paper describes a
new high-density broadband array deployed at significant depths.

While observing ground motions at or near the Earth's surface has generally been acceptable, there are a number of reasons why observations at deeper depths, particularly from an array of instruments, would potentially be useful. It is well known that most seismic 'noise' is generated near the surface and that this noise generally decreases significantly with depth [Levin and Lynn 1958; Forbes 1965; Green et al. 1965; McNamara and Buland 2004]. Observations at depth therefore have the potential to have higher signal-to-noise ratios, and therefore may more accurately measure the elastic waves arriving from any source. The second main reason that seismic measurements at depth could be advantageous is that Earth structure is most heterogeneous in the highly weathered near-surface layers [e.g. Boore and Joyner 1997]. The weathered layer universally has slower seismic velocities, and the heterogeneity caused by variability in weathering makes it nearly always a strongly scattering medium. Since nearly all observations contain this complexity, it is not known precisely how severe the effect is, but it is expected that observations far away from such heterogeneities are simpler and more predictable. Data from the experiment described here has potential for improving insights on the near-surface scattering problem.

In addition to illuminating fundamental questions on seismic wave propagation, seismic measurements at depth are also of interest in the field of gravitational-wave astrophysics. The Laser Interferometer Gravitational-wave Observatory (LIGO) recently announced the first direct detections of gravitational waves produced in a merger of binary black hole systems [Abbott 2016a, Abbott 2016b], hence ushering a new field of inquiry in astrophysics. To fully explore the scientific potential of this field, more sensitive detectors are being designed such as the Einstein Telescope [Punturo 2010] and the Cosmic Explorer [Abbott 2017]. One of the limiting noise factors in these detectors at frequencies below 10 Hz is the seismic noise that causes fluctuations in the local gravitational field. It is expected that this noise source will be reduced underground due to the suppression of seismic surface waves. However, the dependence of this suppression factor on depth is currently not understood, and the optimal configuration of the underground gravitational-wave detectors is unknown. Underground seismic measurements are therefore needed to quantify these effects, thereby directly informing the design of future generations of gravitational-wave detectors.

To explore the promise of subsurface seismological observations, both for geophysical and astrophysical applications, we built and operated an underground three-dimensional (3D) array at the Homestake Mine in Lead, SD. Homestake was one of the largest and deepest gold mines in North America. It officially closed operations in 2002, but reopened in 2007 as the Sanford Underground Research Facility (SURF), and currently supports several other experiments, including dark matter and neutrino experiments that benefit from the cosmic ray shielding of the rock overburden. The significant infrastructure in the Homestake Mine, including easy access to numerous underground levels with hundreds of kilometers of available drifts, availability of power and digital network infrastructure, and safety protocols and the SURF infrastructure made the Homestake Mine an ideal location for the development of a 3D seismometer array.

In this paper, we describe the novelty of the 3D Homestake array as compared to other subsurface seismological deployments, the experience learned in operating the underground array for 2 years, and preliminary results that demonstrate the potential of these data for additional research in the future.

SEISMOMETER ARRAY

The Homestake seismometer array, depicted in Figure 1, consisted of 24 seismic stations: 15 stations underground and 9 on the surface. The locations of stations are known with uncertainties on the order of 1 m based on precise surveys for past mining operations provided by SURF. Underground station locations were obtained from these maps. Surface station coordinates come from long-term averages of GPS data. All of the underground stations were installed between December 2014 and March 2015, and remained operational until December 2016. The surface stations were installed in May 2015 and remained operational until September 2016. The seismic equipment used in the experiment was provided by the Portable Array Seismic Studies of the Continental Lithosphere (PASSCAL) instrument center, which is a part of the Incorporated Research Institutions for Seismology (IRIS). Most stations used Streckheisen STS-2 high-sensitivity broadband seismometers. The exceptions were the underground station on the 300-ft level and three surface stations, where we deployed the more water resistant Guralp CMG-3T seismometers.

The underground stations were scattered across several levels: one at a depth of 300 ft (91 m), one at 800 ft (244 m), one at 1700 ft (518 m), five at 2000 ft (610 m), three at 4100 ft (1250 m), and four at 4850 ft (1478 m). The locations of these stations were chosen to maximize the horizontal aperture of the array within the constraints imposed by safe access, availability of power, and access to SURF's fiber optic network. In several cases, we had to extend existing power and network cables to support the stations. We strove to locate sites as far as possible from activity in the mine and from water drainage pathways. Stations were usually placed in alcoves or blind alleys to minimize the effects of the air drifts, although several stations were installed in enlarged areas within the main drifts of the mine. In most cases, we found there were complex tradeoffs between cost of installation and distance from active operations.

Many sites had existing concrete pads of various sizes and thicknesses from the original mine operation. When necessary we poured a concrete pad directly onto the rock. In all cases a granite tile was attached to the pad using thinset mortar. All underground site preparation was completed three (or more) months prior to the installation of the instruments. Each seismometer was placed directly onto the granite tile, and was oriented to cardinal directions using an Octans gyrocompass from the IRIS-PASSCAL instrument center [Ekstrom and Busby 2008]. To reduce noise induced by air flow we covered each sensor with two nested huts constructed of 2" thick polyisocyanurate foam panels and sealed with foam sealant. The digitizer was placed several meters away, and included a Quanterra Q330 data logger, a baler, and network and power supply electronics. Each station was powered by a small 12V battery continuously charged by a simple AC charger. The battery provided approximately a one day power reserve, which proved more than adequate to cover any power outages encountered during the experiment.

In addition to saving the data locally with a baler, we utilized real-time telemetry for all underground sites and six of the nine surface sites. The underground stations were synchronized using a custom-designed GPS optical distribution system. The GPS signal was received by a GPS antenna mounted on the roof of the SURF administration building and piped to a Q330 in the server room of the same building. This "master" Q330 data-logger was used to convert the received high-frequency GPS signal into the separate 1PPS (1 pulse-per-second) and NMEA metadata components that were used as an external timing signal for the underground instruments. The output from the master Q330's EXT GPS port was fed into an electro-optical transceiver to convert the analog voltage output to optical signals. The transceivers were custom-made for this application by Liteway, Inc. (model number GPSX-1001). An optical-fiber network of optical splitters and transceivers was installed underground to distribute this GPS timing signal to all underground stations, while maintaining its signal-to-noise ratio throughout the mine. At each station, a transceiver was used to convert the optical signals back to electrical, which were then sent into the Q330's EXT GPS port. Phase errors logged by the Q330 digitizers suggest the timing precision achieved with this system was of the order of 1 µs. Systematic errors from propagation and electronic delays were negligible.

Five of the nine surface stations were located on SURF property above the underground stations. Another station was located at Lead High School (LHS) in collaboration with the Lead Deadwood Public School District. We deployed the remaining three stations on private land in an outer ring at a nominal radius of 5 km from the array center. We used conventional, portable broadband sensor vaults but carefully separated the wall of the sensor vault from the concrete pad poured at the bottom. This detail is known from early experience in the 1990s at IRIS-PASSCAL to reduce tilt noise from soil motions. All but one of the sites (DEAD) were bedrock sites with a concrete pad poured on weathered metamorphic rocks of variable lithologies. The surface stations were all oriented by conventional compass methods, which means the precision is less than the underground sites oriented with the Octans instrument. We insulated the sensor vault with a layer of foam and burial with as much of a soil cover as possible. We had the common problem of rain washing some cover away that we restored when the instruments were serviced.

While the three outer stations were stand-alone, the remaining six inner stations all used radio telemetry. Of these, the LHS site located near the high school used a point-to-point radio that linked the outdoor site to a Linux computer in a computer laboratory at the school. The remaining five stations were radio-linked to a master radio on the roof of the SURF administration building where our data logging computer was located. All surface sites except LHS used solar power; LHS used an AC system similar to underground sites but with a larger battery backup. All surface sites used the standard Q330 GPS timing system.

The telemetry system we deployed used a computer running the Antelope software [e.g., Malone 1999; BRTT 2017] at the SURF administration building to handle real-time communication to all underground sites and five of the nine surface sites. We ran a separate Linux computer running Antelope at LHS to handle real-time communications

with that single site. This approach was necessary to deal with firewall issues at both SURF and the high school. We then set up an orb2orb feed to a University of Minnesota computer that acted as a data concentrator. The participating institutions and the IRIS-DMC were then able to tap that connection for real-time feeds with a latency of a few tens of seconds. We developed a custom monitoring system to automatically test for a range of conditions and build web-based quality control summaries. We also set up a rotating shift schedule to monitor this diagnostic information on daily basis. This allowed us to quickly identify and diagnose problems. This was a major factor in the very high data recovery rate of this experiment (near 100% for every site except DEAD, which had power problems in the winter of 2015-2016 and also had a corrupted E-channel response). Furthermore, the telemetry data have no mass position related issues except for two sensors failures. In addition, this quality control monitoring allowed us to detect and diagnose a subtle problem on station E2000. This station began showing odd tilt transients, which were tracked down to failure of the thinset grout on the base of one of our granite tiles. This was repaired by pouring a new concrete pad and setting the tile directly on the concrete.

PRELIMINARY RESULTS

The primary novelty of the Homestake Array is that it is a three-dimensional broadband array, approximately spanning a cubic volume that is 1.5 km on each side (and hence a volume of about 3.4 km^3), in a relatively seismically quiet and geologically stable region. This unusual array configuration leads to both unique opportunities and challenges. Here, we provide preliminary analyses that demonstrate some of the potential prospects and issues. We first describe the ambient noise levels of the stations in our array, which at some periods are exceptional. We then describe seismic events detected with our array that demonstrate the kinds of event data that were collected in this experiment. As expected for an array of such small aperture, waveforms have a very high degree of coherence, but there are subtle differences between stations at depth and those nearer to the surface that suggest more detailed analysis may yield fruitful information regarding near-surface heterogeneity. Finally, since the results presented here represent only initial work on this dataset, we discuss possible future applications of these data.

Noise Spectra

The ambient seismic noise levels at the Homestake mine, especially at the deepest levels, are remarkably low and stable. We demonstrate this by computing the displacement amplitude spectral density (ASD) of seismic noise over long periods, for different stations and for different seismic channels (east, north, vertical). We use all available data (from January 2015 to December 2016), split into 900 second intervals. The median amplitudes in each frequency bin for the east-west seismic channel are shown in Figure 2 in comparison to the low- and high-noise models of Peterson [1993]. The left panel compares the ASDs for stations at several different depths. All of the stations are in close agreement in the middle range of frequencies (0.1-0.5 Hz), which corresponds to the microseismic peak. At higher frequencies, there is significantly less noise with depth: above 0.5 Hz, the stations at 4100 ft and 4850 ft depths are nearly an order of magnitude

quieter than other stations. At the lowest frequencies (<0.1 Hz), there is also a good agreement between the stations, although a slight increase in noise is apparent at the surface stations; this may be due to larger temperature variations closer to the surface that induce tilts in the concrete pads. While the underground stations at any given depth tend to agree very well, there is a wide range of variability among the surface stations, as depicted in the right panel of Figure 2. This is due to differences in the local environment in terms of thermal insulation and proximity to human activity.

Figure 3 shows ASD histograms for the RRDG surface station (left) and for the A4850 underground station (right) as examples of a representative surface station and our deepest and most isolated underground station. Here, the histograms of ASDs are calculated from 400-second data intervals over 1 year in each frequency bin, revealing the overall variability of the seismic noise at each station. The white curve represents the median ASD (identical to those shown in Figure 2), the black curves represent the 95% confidence intervals in each frequency bin, and the color scale shows the overall distribution. The Peterson low- and high-noise models are shown in dashed gray.

The histograms display about two orders of magnitude of variation across all frequencies for both the RRDG station and the A4850 station. The A4850 station measures less noise in general and appears to have less overall variation than RRDG. There also appears to be significantly more high-frequency noise in the RRDG station, potentially due to wind-generated or anthropogenic surface waves that are suppressed with depth. Both stations stay within the low- and high-noise Peterson models most of the time. However, in the 0.3–0.9 Hz range the A4850 station is actually below the low-noise model a significant fraction of the time. We also observe a considerable difference between the vertical channel and the horizontal channels at low frequencies. At 0.01 Hz and below, the vertical channels on both stations have almost an order of magnitude lower noise than the horizontals, due to tilt noise that increases with period on horizontal components [Wielandt, 2002]. On the other hand, the horizontal components of many of the underground sites are very quiet, even down to tidal frequencies.

The low-noise levels of a significant fraction of our stations at depth suggests that the array may be useful for better understanding how ambient noise levels depend on depth, and in particular what fraction of the noise is spatially and temporally coherent. Such a study, which cannot be done with a single borehole seismic station, is beyond the scope of this contribution, but is expected to be discussed in future contributions.

Event Detection and Waveform Observations

Detecting and analyzing seismic events in an area with otherwise sparse station coverage using our small-aperture array of 24 ultra-quiet sites was technically challenging since conventional automated detectors typically assume all sites provide equally weighted independent data. Thus, attempts at automatic detection using Antelope 5.6 [Malone 1999; BRTT 2017] applied to our array data augmented by data from 8 regional stations (see Fig. 4b) resulted in a large number of spurious detections. We solved this issue, and reduced the false detection rate to near zero, by running the detection algorithm only on

Commented [VCT2]: Why is the Deadwood station so good? It looks to be nearly identical to A4850, or even better. Is the lack of (7s) microseism related to it dying (not recording) in the winter? If so, that would be slightly misleading.

Commented [PMM3R2]: I'm not sure. There are a few possibilities. I'll take a look at the DEAD data and see if maybe there was something I missed.

the three outer surface sites (DEAD, TPK, and SHL), one of the quietest underground sites (D4850) and the 8 regional stations, and by requiring six P-wave associations before declaring an event. These choices resulted in significantly raising the detection threshold, and no longer detecting events from a local active surface mine, located only 2.5 km west of station TPK. A large number of such very local events exist (see Fig. 5 for one example), indicating at least one blast per day during the workweek, and could be used in future studies. For example, Figure 5 clearly shows the theoretically expected suppression of Rayleigh waves with depth, with Rayleigh waves barely visible on any of the stations in the 4000s subarray.

Standard analyst review of the revised detection routine applied to six months of data (January-July 2015) resulted in the detections shown in Figure 4. Of the 431 epicenters, 359 are in the local area shown in Fig. 4b and 72 are at regional to teleseismic distances shown in Fig. 4a. The locations shown in Fig. 4a were produced by association of events with those from the U.S. Geological Survey catalog [ANF 2017] and using the associated epicenters. Locations in Fig. 4b were estimated with the dbgenloc program [Pavlis et al. 2004] assuming the IASPEI91 earth model. All of the 359 local events in Fig. 4b are likely to be coal mining explosions from the Powder River Basin in eastern Wyoming. All have similar waveforms with emergent P waves and prominent surface waves like the event shown in Figure 5. Despite assuming fixed depths (of zero), some epicenters were poorly constrained and likely badly estimated due to too few of the regional stations having observable P or S waves. Most well located events cluster in the coal mining district, supporting our hypothesis that these are mining related.

Figures 6 and 7 show three-component subarray stacks for two representative events. Since we found systematic differences in waveforms with sensor depth, these subarray stacks were grouped into three subarrays defined in Figure 5 ('Surface', '2000s' and '4000s'). Note that we treated the 300 and 800 stations as part of the 'Surface' subarray, grouped the 1700 station with the five 2000-level stations in the 2000s subarray, and grouped the 4100 and 4850 stations in the 4000s subarray. Such systematic differences are expected due to near-surface effects that have been known to complicate seismic array processing since the early VELA UNIFORM experiments of the 1960s (REFERENCES). To produce each subarray stack, we used an array-based cross-correlation algorithm to align signals prior to stacking [Pavlis and Vernon 2010]. Typical correlation window lengths were 2-4 s for the local mining blasts and 10-20 s for the teleseismic events. The stacked signals of the 3 subarrays were then manually aligned to produce the figures shown.

Figure 6 shows subarray stacks from an intermediate depth event in Alaska where the pP phase is significantly bigger than P.   Nonetheless, the P signal shown magnified in Figure 6b has a very high signal-to-noise ratio and a relatively high frequency content for a teleseism. Figure 7 shows comparable results for a typical, larger Powder River Basin mining explosion. The subarray stacks show significant differences in waveforms that are unquestionably not related to background noise. Figure 7 shows a secondary amplitude effect not seen in the teleseismic waveforms. In particular, there is a strong change in amplitude with depth, with the average surface-station P wave roughly a factor of 2

higher amplitude that the 4000s subarray average. A comparable difference in P-wave amplitude is not seen for the teleseismic signal in Figure 6. How much of that difference is due to the differences in emergence angle (steep angle of incidence for the teleseism but approximately horizontal for the mining explosion) and how much of the difference is due to frequency content (upper limit around 2 Hz for the teleseism and upper limit near the 40 Hz antialiasing frequency corner for the mining explosion) is not yet clear.

These results, though preliminary and exploratory, further demonstrate the potential of the Homestake array dataset to be used to explore the role of near-surface structure in complicating earthquake waveforms. Unlike surface arrays, where the complexity of near-surface structure is convolved with complexity of earthquake sources, the Homestake array's geometry allows for separate evaluation of these two aspects of earthquake waveform modeling. While some of this separation is possible with single borehole arrays, the linear geometry inherent in such arrays is a clear drawback, leading to significant underdetermination of inversions, to which the Homestake array data should be less susceptible.

CONCLUSIONS AND FUTURE DIRECTIONS

We have described a three-dimensional array of high-sensitivity broadband seismometers in the Homestake mine, SD, spanning roughly a cubic mile underground. We have also shown preliminary results of analyses of data acquired by this array. The data are characterized by exceptionally low seismic noise levels that are also very stable over a year-long time scale. The data also contain high signal-to-noise records of hundreds of transient signals due to local or regional mining blasts, due to teleseismic events, and due to active excitation experiments performed at the surface and underground. A preliminary look at these transient events reveals rich structure in terms of depth dependence of different wave components, and in terms of interaction of waves with the surface.

We further expect the unusual array geometry to be useful for a number of analyses in addition to the two examples provided. Several such studies are already underway, and here we briefly describe some of these possibilities, which will be subjects of future publications.

In the analysis of ambient noise, the depth extent of the array may be useful in helping estimate the directionality and modal content of the seismic noise. For example, the depth dependence of the Rayleigh and Love eigenfunctions can be directly measured from Homestake data and then used as a constraint on the observed seismic noise modes, hence avoiding common assumptions about the dominance of fundamental-mode surface waves. Combined with other radiometer-based techniques used in other areas of physics [Thrane et al. 2009], such estimates would directly contribute to the design of future underground gravitational-wave detectors.

For teleseismic earthquake analysis, other analyses beyond what was described above may also help understand the scattering and reflection of the nearly-vertical incoming waves with the surface, hence directly measuring the impact of the surface weathered

layer on the teleseismic waveforms. One example that is being pursued relates to how well one station's waveforms can be predicted based on knowledge of all other stations' data. The dependence of station location on the success of such predictions should provide valuable information about the heterogeneity of subsurface structure.

Finally, comparison of P-wave particle motions within the array may yield unique data on P-wave anisotropy. The rocks at Homestake are predominately highly foliated phyllites and schists [REF] and are known to be highly anisotropic [REF]. It is thus not surprising that most of the events we have examined (e.g., Fig. 6 and 7) show significant amplitudes on the transverse component, even during the first cycle of the P wave. Further analysis will be necessary to fully identify how strongly anisotropy affects observed waveforms.

> **Commented [VM6]:** References from Gary?

References

Abbott, B. P. et al. (The LIGO Scientific Collaboration and Virgo Collaboration) (2016a), Observation of Gravitational Waves from a Binary Black Hole Merger, *Physical Review Letters* **116**, 061102.

Abbott, B. P. et al. (The LIGO Scientific Collaboration and Virgo Collaboration) (2016b), GW151226: Observation of gravitational waves from a 22-solar-mass binary black hole coalescence, *Physical Review Letters* **116**, 241103.

Abbott, B. P. et al. (The LIGO Scientific Collaboration and Virgo Collaboration) (2017), Exploring the sensitivity of next generation gravitational wave detectors, *Classical and Quantum Gravity* **34**, 044001.

Abercrombie, R.E. (1995). Earthquake locations using single-station deep borehole recordings: implications for microseismicity on the San Andreas Fault in southern California, *J. Geophys. Res.,* **100**, 24003-24014.

ANF (2017). Array network facility of USArray website, http://anf.ucsd.edu/events/, latest access April 27, 2017.

Boore, D.M. and W.B. Joyner (1997). Site amplifications for generic rock sites, *Bull. Seismol. Soc. Am.*, **87**, 327-341.

BRTT (2017). Boulder real time technologies website, http://brtt.com, latest access April 25, 2017.

Ekstrom, G., and R.W. Busby (2008). Measurements of seismometer orientation at USArray Transportable Array and backbone stations, *Seismol. Res. Lett.*, **79**, 554-561.

Forbes, C. B. (1965). The LASA sensing system design, installation, and operation, *Proceedings of the IEEE,* 53(12), pp. 1834-1843.

Gibowicz, S.J., R.P. Young, S. Talebi, and D.J. Rawlence (1991). Source parameters of seismic events at the underground research laboratory in Manitoba Canada: scaling relations for events with moment magnitude smaller than -2, *Bull. Seismol. Soc. Am.*, **81**, 1157-1182.

Green, P. E. (1965). Principles of an experimental large aperture seismic array (LASA), *Proceedings of the IEEE (0018-9219),* 53 (12), p. 1821-1833.

IRIS (2017). Incorporated Research Institutions for Seismology metadata aggregator website, www.iris.edu/mda, latest access July 12, 2017.

Lay, T. and T.C. Wallace (1995). Modern global seismology, Academic press, San Diego.

Levin, F. K., and R. D. Lynn (958). Deep-hole geophone studies, *Geophysics,* **23**, 639-664.

Ma, K.-F., Y.-Y. Lin, S.-J. Lee, J. Mori, and E.E. Brodsky (2012). Isotropic events observed with a borehole array in the Chelungpu Fault Zone, Taiwan, *Science*, **337**, 459-463.

Malone, S. (1999). Seismic network recording and processing systems I, *Seismol. Res. Lett.*, **70**, 175-178.

McNamara, D.E. and R.P. Buland (2004). Ambient noise levels in the continental United States, *Bull. Seismol. Soc. Am.*, **94**, 1517-1527.

Nadeau, R.M. and T.V. McEvilly (1997). Seismological studies at Parkfield V: characteristic microearthquake sequences as fault-zone drilling targets, *Bull. Seismol. Soc. Am.*, **87**, 1463-1472.

Okada, Y., S. Hori, K. Obara, S. Sekiguchi, H. Fujiwara, and A. Yamamoto (2004). Recent progress of seismic observation networks in Japan – Hi-net, F-net, K-NET and KiK-net, *Earth Planets Space*, **56**, xv-xxviii.

Pavlis, G. L. and F. L. Vernon (2010). Array processing of teleseismic body waves with the USArray, *Computers and Geosciences*, **36**(7) , pp. 910-920.

Pavlis, G. L., F. L. Vernon, D. Harvey, and D. Quinlan (2004). The generalized earthquake location (GENLOC) package: A modern earthquake location library, *Computers in Geosciences, 30*, 1079-1091.

Peterson, J. (1993). Observations and modeling of seismic background noise, *USGS Open-File Report*, **93-322**.

M. Punturo et al. (2010), The third generation of gravitational wave observatories and their science reach, *Classical and Quantum Gravity* **27**, 084007.

Richardson, E. and T. Jordan (2002). Seismicity in deep gold mines of South Africa: implications for tectonic earthquakes, *Bull. Seismol. Soc. Am.*, **92**, 1766-1782.

Stein, S. and M. Wysession (2003). An introduction to seismology, earthquakes, and earth structure, Blackwell publishing, Malden MA.

Thrane, E., et al. (2009). Probing the anisotropies of a stochastic gravitational-wave background using a network of ground-based laser interferometers, *Phys. Rev. D*, **80**, 122002.

Wielandt, E. (2002). Seismic sensors and their calibration, in *New Manual of Seismological Observatory Practice (NMSOP), Vol. 1, Chap 5, ed.* P. Bormann, IASPEI, Potsdam, Germany.
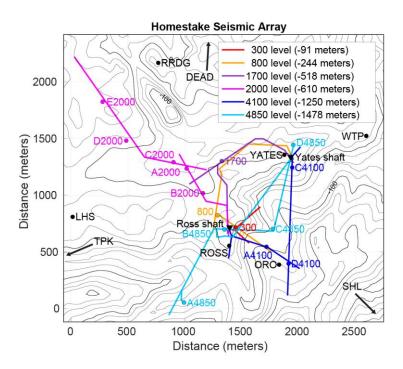
Figures

Figure 1: Homestake seismometer array layout. The lines of different colors depict the relevant drifts at various depths, along which we installed underground seismic stations. The black filled circles denote the surface stations (remote surface stations DEAD, SHL, and TPK were located approximately 2-3 km outside the depicted region). Also shown are the two shafts at the Homestake mine, known as the Yates and Ross shafts, denoted by black filled triangles.
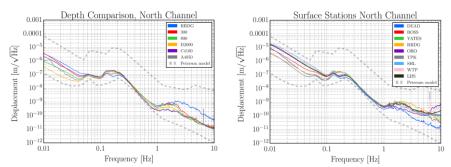
Figure 2: Median amplitude spectral densities for Homestake seismic stations. Numbered legend entries denote depth in feet, while numberless legend entries denote surface stations. Peterson low- and high-noise models are shown as dashed gray lines. See text for more detail.
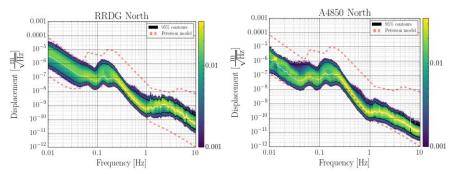

Figure 3: Histograms of amplitude spectral density in each frequency bin for a surface station (left) and for an underground station at 4850 ft depth (right). Median ASDs (solid white), 95% confidence intervals for each frequency bin (solid black), and the Peterson low- and high-noise models (dashed gray) are shown. See text for more details.
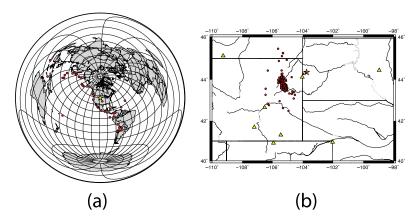
(a)   (b)

Figure 4: Epicenter maps of events recorded by Homestake 3D array. (a) An azimuthal equal distance projection map centered at the array site marked with a star. Epicenters of distant earthquakes recorded by the array in the 2015 study period are shown as circles. (b) Epicenter map focused on local and regional events. The array location is again shown as a star and estimated event epicenters are shown as circles. Black filled triangles are regional stations used for detection and location of the events plotted.
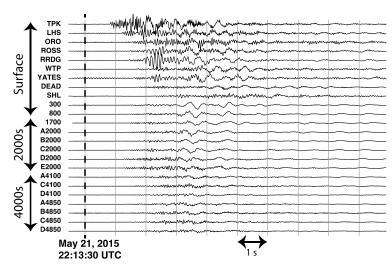

Figure 5: Vertical component seismograms from local surface mine. Seismograms are displayed at true amplitude and grouped by subarrays used throughout this paper. Records for each subarray are sorted by epicentral distance from the estimated source location (approximately 4 km west of TPK). Subarrays are ordered by increasing depth.
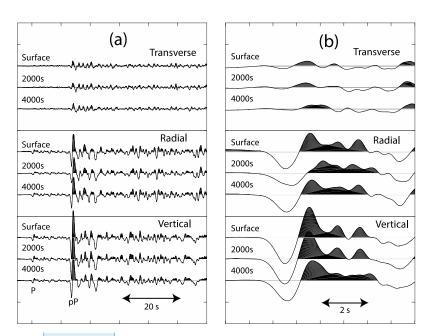
Figure 6: Displacement [? Velocity?] seismograms from an Alaskan earthquake recorded by the Homestake 3D array. Panel (a) illustrates the three components of subarray stacks defined in the text. It shows the first 2 minutes of the data following the P wave signal. These data were filtered with a 0.01 to 2 Hz bandpass filter before stacking. The P wave of this event is much smaller than the pP phase seen approximately 25 s after P (event depth is 120 km and distance is 33°). Panel (b) shows a shorter time window focused on only the P wave (6 s following measured P time). All plots are true amplitude meaning amplitudes differences between seismograms are real. In all figures the seismograms have been aligned by cross correlation before stacking. Stacks are aligned manually.

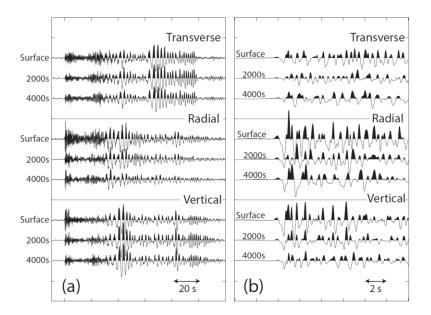Commented [VCT7]: Gary, please confirm which it is.

Figure 7: Seismograms from a typical Powder River Basin coal mining explosion recorded by the Homestake 3D array. All the data shown in this figure were filtered with a 5 pole Butterworth filter with a pass band from 0.25 to 10 Hz. Panel (a) shows 2 minutes of data following P-wave and is directly comparable to Figure 6a. Panel (b) is directly comparable to the Figure 6b but for this explosion source instead of a teleseismic earthquake. Panel (b) shows subarray stacks for 6 s of data following the measured P wave time. Note that the 2000s subarray is oriented roughly in the direction of propagation of the P-wave for this event. All figures show seismograms in true amplitude and seismograms were again aligned by a mix of cross-correlation and manual picks as described in the text.